IEEE Access
Multidisciplinary | Rapid Review | Open Access Journal

Received July 10, 2020, accepted July 30, 2020, date of publication August 12, 2020, date of current version August 25, 2020.

Digital Object Identifier 10.1109/ACCESS.2020.3016118

Risk Assessment Model for UAV Cost-Effective Path Planning in Urban Environments

XINTING HU[1], BIZHAO PANG[2], FUQING DAI[1], AND KIN HUAT LOW[3], (Member, IEEE)

[1]School of Air Traffic Management, Civil Aviation University of China, Tianjin 300300, China
[2]Air Traffic Management Research Institute, Nanyang Technological University, Singapore 637460
[3]School of Mechanical and Aerospace Engineering, Nanyang Technological University, Singapore 639798

Corresponding author: Kin Huat Low (mkhlow@ntu.edu.sg)

This work was supported in part by the National Key R&D Program of China under Grant 2016YFB0502400, and in part by the UAS Programme in the Air Traffic Management Research Institute (ATMRI), Nanyang Technological University (NTU), Singapore.

ABSTRACT Increasing use of Unmanned Aerial Vehicle (UAV) in urban environments poses to an increased risk of fallen UAVs impacting people and vehicles on the ground, as well as colliding with manned aircraft in the vicinity of airports. Risk management of UAV flights for safe operations is essential. We proposed a comprehensive risk assessment model for UAV operation in urban environments. Three risk categories (people, vehicles, and manned aircraft) were considered and each risk cost was quantified using collision probability. We adjusted the risk costs in various magnitudes to a same scale and conducted a sensitivity analysis to determine the optimal coefficients of the three risk cost models. We then computed the total risk and generated a risk cost map for path planning. Modified path planning algorithms were used to produce a cost-effective path, and we compared their performances in terms of total risk cost and computational time. Lastly, we performed simulations to validate the feasibility and effectiveness of our proposed risk assessment model. The results show that the risk-cost-based path planning method can generate safer path for UAV operations than the traditional shortest-distance-based method. Our proposed model can be extended to complex urban environments by including more relevant parameters and data.

INDEX TERMS Unmanned aerial vehicle, risk assessment model, risk cost map, path planning, urban environments.

I. INTRODUCTION

The UAV industry has been growing in recent decades. UAVs are used for various purposes in urban environments, such as traffic monitoring [1], photography, and weather forecasting [2]. They are also a core component of Urban Air Mobility (UAM) [3] and plans for smart cities in the near future [4], [5].

However, the increase in UAV operations in urban low altitude airspace may increase the risk of drone accidents. UAVs in urban areas may fall and hit people and vehicles on the ground [6], [7]. UAVs may also intrude into airport airspaces [8]. An aspect of safe UAV operations would be to prevent UAVs from flying over high risk areas, such as densely populated areas and airports.

Geofencing is one way to do so [9]. Airspace can be segregated into different risk areas, and UAVs would only be allowed to operate in designated safe airspace. However, this is not feasible in cities like Singapore [10] where available airspace for UAV operations are already very limited.

An alternative way would be by airspace utilization – using risk cost map for UAV path planning to avoid high-risk areas. The concept of risk cost and risk cost map has been studied in safety management and risk assessment [11], [12], and some researchers have introduced risk cost map into UAV path planning [13]–[15]. Primatesta *et al.* [13] proposed two algorithms for UAV path planning based on risk awareness to tackle dynamic risks and threats in operation environments. Primatesta and another team [14] studied the possible risk factors in urban environments for UAV operation. Wu *et al.* [15] proposed a 4-D UAV path planning method based on risk cost map to enable UAV to fly along the cost-effective path. However, these papers focus on designing UAV operation rules and do not model risk events related to urban characteristics.

Some researchers have studied obstacles, weather conditions, and other vehicles on the ground [16]–[18] as possible threats. In urban environments, however, additional threats have to be taken into consideration for risk-based path

The associate editor coordinating the review of this manuscript and approving it for publication was Yang Tang.

planning. These include people and vehicles on the ground, and manned aircraft in airport areas. Other researchers have conducted population-related risk assessment for UAV path planning in terms of emergency landing [19], and trade-off between population risk and flight cost [20]. However, few researchers have considered the threats of falling UAV impacting ground vehicles, UAV entering controlled airspace and colliding with manned aircraft, or incorporating all these risks to generate a risk cost map for the complex urban environments.

Apart from the risk assessment models, another challenge is the method for risk-based path planning. Existing methods are based on graph search algorithms (such as Dijkstra algorithm [21], heuristic A* algorithm [22], genetic algorithm [23]) or sample-based ones (such as Probabilistic Roadmaps [24], Rapidly-exploring Random Trees (RRT) [25]). As a global optimization algorithm, ant colony algorithm [26] also performs well in UAV path planning problems. However, traditional algorithms, like A* and ACO, often encapsulate the distance in the heuristic function and may not consider the risk a path contains.

To address the gaps in the literature mentioned above, a risk assessment model and risk-based path planning method is proposed in this paper. Our main contributions of the present work are listed as follows:

(1) We develop risk models for UAV collision with people on the ground, vehicle, and manned aircraft. Expected fatalities, collision frequency, population density, distribution of ground vehicle, as well as UAV performance parameters are considered in the modelling of different risk costs.

(2) We propose a comprehensive risk assessment model. The model incorporates evaluation standards and sensitivity analysis on risk coefficients to quantify multiple risks in urban environments.

(3) Three path-planning algorithms are used and compared in this work to generate paths with low risk cost and to evaluate their strengths and weaknesses in different scenarios.

The rest of this paper is organized as follows:

- Section II presents the overall methodology of this work.
- Section III presents the risk cost modellings.
- Section IV presents the path planning method and algorithm.
- Section V presents the simulation studies and results.
- Section VI provides a summary of our work.

II. METHODOLOGY

The overall framework of the paper is presented in Figure 1. Our risk assessment models generate a risk cost map, which can then be used to plan the risk-cost-effective path. Simulations with different situations and combinations of risk types are presented to demonstrate the feasibility and effectiveness of proposed models.

As depicted in Figure 1, there are four steps for the modelling of risk cost map. First, we analyze risks in urban environments where UAV operates. Three risks are considered: UAV impacts people on the ground, UAV impacts ground vehicles, and UAV collides with manned aircraft in the vicinity of airports. Second, we develop three risk assessment models to quantify the costs of each risk. Third, we aggregate all the three risk costs as a total cost value. Fourth, we generate risk cost map. Selected urban areas are meshed and the risk cost of each cell will be computed and presented in the map.

With the risk cost map, the UAV cost-effective path planning will be developed by using algorithms of standard Dijkstra, modified A*, and modified ACO. Instead of minimizing the total distance, the objective of the proposed algorithms is to find the risk-cost-effective path.

We conduct two groups of simulations to verify the feasibility of proposed models. The first group involves simulations of UAV path planning in different situations considering all three risks. The second group involves four simulations with different combinations of the three risk types to help us understand the influence of risk cost type on the result of cost-effective path. We will discuss the analysis of the simulation results at the end of this paper.

III. RISK ASSESSMENT MODELS

This section describes the concept of risk cost map. We analyzed and modelled the derived risks in urban environments, with two caveats:

(i) The risk of UAV impacting ground buildings is not considered in this study;

(ii) The density of people on the ground, vehicles and UAV are regarded as uniform distribution.

Three main risks are considered: people on the ground, vehicles, and manned aircraft. The risk cost map incorporates all three risks.

Figure 2 shows an example of path planning based on a risk cost map. The map is formed with links and nodes. Each link has a risk cost value computed according to the risk severity within the specified area. The risk cost value is presented in a colour spectrum, with red representing a high risk cost and blue representing a low risk cost. The arrow with a solid line shows the path with the shortest distance from origin to destination. The arrow with a dashed line is the cost-effective path. This path avoids the high-risk cost areas and has a risk cost that is much lower than the path with the shortest distance.

The key objective of our work is to model and generate the risk cost map, then producing the cost-effective path using modified algorithms.

A. RISK MODEL PERTAINING TO PEOPLE

UAVs in the air may lose control or power and fall to the ground, potentially hurting people below (see Figure 3). We modelled the risk cost of a UAV hitting people on the ground according to the three components of a crash incident: (a) a UAV malfunctions and falls; (b) the UAV impacts people on the ground; and (c) the people on the ground injured by the UAV.

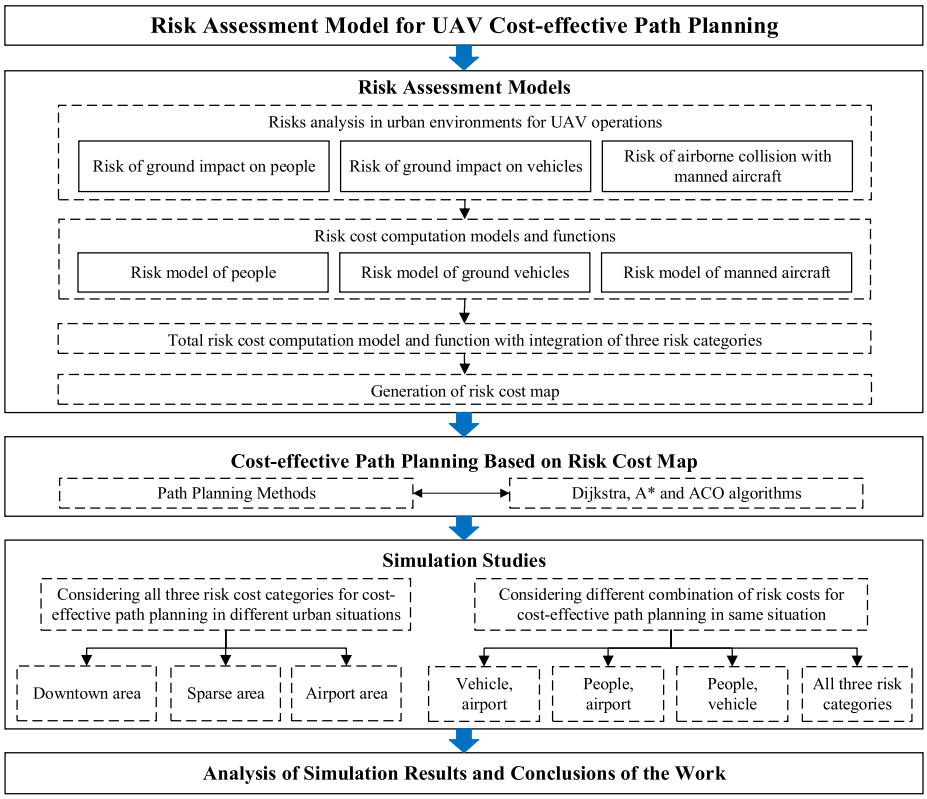

FIGURE 1. Overall framework of the proposed work presented in this paper.

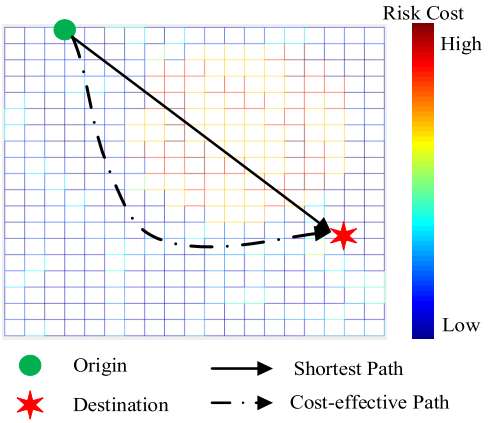

FIGURE 2. Illustration of risk cost based path planning showing a cost-effective path generated by avoiding the high risk cost area.

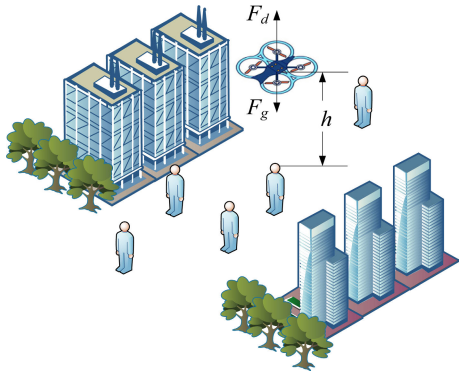

FIGURE 3. UAV above people on the ground.

The expected fatality of UAV impacting people is defined as the number of fatalities per hour as given by

$$P_{\text{event}-1} = P_{\text{people}} = \lambda MF \tag{1}$$

where $P_{\text{event}-1}$ is the expected fatality of event 1 associated to people on the ground in the present work, λ is the probability of crashing UAV per flight hour, M is the number of people hit by falling UAV, and F is the fatality rate associated to the function of kinetic energy, i.e. falling height and weight of the UAV.

The number (M) of people hit by falling UAV in Eq. (1) is the variable of population density, defined as

$$M = A\rho_P \tag{2}$$

where A is the exposed area in which UAV hitting the ground, and ρ_P is the population density.

The vertical force of falling UAV can be evaluated by [27]

$$F_d = \frac{1}{2} R_I A \rho_A v_{rel}^2 \tag{3}$$

where R_I is the drag coefficient related to the UAV type, ρ_A is the density of air, and v_{rel} is the actual air speed of falling UAV.

TABLE 1. Sheltering coefficients (values extracted from [14], proportionally).

c_s	Sheltering
0^+	No obstacles
0.25	Sparse trees
0.50	Trees and low buildings
0.75	High buildings
1	Industrial buildings

Then the acceleration of UAV is

$$a = \frac{F_g - F_d}{m} = g - \frac{R_I A \rho_A v_{rel}^2}{2m} \tag{4}$$

where F_g is the gravitational force, $F_g = mg$.

The velocity of UAV hitting on the ground is

$$v = \int_0^t \left(g - \frac{R_I A \rho_A v_{rel}^2}{2m} \right) dt = \sqrt{\frac{2mg}{R_I A \rho_A}} \left(1 - e^{-\frac{hR_I A \rho_A}{m}} \right) \tag{5}$$

where h is the falling height of UAV above the people on the ground.

The impact kinetic energy of the falling UAV is known as

$$E_{imp} = \frac{1}{2} m v^2 \tag{6}$$

A sheltering coefficient c_s considers the buffering effects of buildings and trees softening the ground impact to people from drones falling out of the sky [14]. By adopting the limits suggested in [28], $c_s \in (0, 1]$, the range takes an average value of 0.5, with higher values meaning better sheltering and a lower probability of fatality for the same kinetic energy.

By incorporating the sheltering effects to the impact kinetic energy, the fatality rate of impact F can be obtained as [28]:

$$F = \frac{1}{1 + \sqrt{\frac{b}{d}} \left(\frac{d}{E_{imp}} \right)^{\frac{1}{4c_s}}} \tag{7}$$

where b is the impact energy that might cause 50% fatality with $c_s = 0.5$, while d is the impact energy threshold required to cause fatality as c_s approaching zero (see Figure 2 in [28]). The values of c_s shown in Table 1 are applied in the present work.

B. RISK MODEL PERTAINING TO GROUND VEHICLES

UAVs may fall and compromise the safety of road traffic (see Figure 4).

Similar to the modelling for people on the ground, there are also three components to a crash incident on road traffic: (a) a UAV malfunctions and falls; (b) the UAV hits a ground vehicle; (c) the crash incident causes a traffic accident which subsequently injuries people.

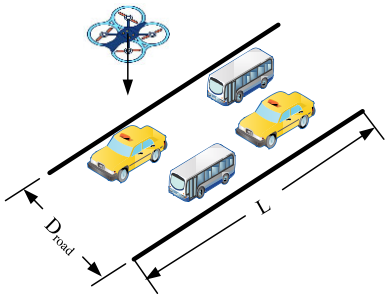

FIGURE 4. UAV above ground vehicles.

The expected fatality of UAV impacting a ground vehicle can be defined as the number of fatalities per hour caused by falling UAVs as

$$P_{\text{event}-2} = P_{\text{car}} = \lambda C T \tag{8}$$

where C is the probability of falling UAV hits a vehicle, T is the number of fatalities caused by the average car accidents.

The probability of UAV hitting a ground vehicle can be defined in terms of the ratio of the total areas of all vehicles projected and the total road area covered. The probability C is expressed as

$$C = \frac{\overline{S_{car}} N}{S_{road}} \tag{9}$$

where $\overline{S_{car}}$ is the vehicle's projected area on ground and N is the number of vehicle. Note that $N = KL$ and $S_{road} = LD_{road}$, where K is the traffic density (the number of vehicles per unit length of road), L is the length of road, and D_{road} is the width of road considered.

C. RISK MODEL OF MANNED AIRCRAFT

The safety issues of collision between manned aircraft and UAV are crucial to the UTM-ATM integration [29]. Thus, we also consider airports as one of the risk areas.

The incidence of collision between manned aircraft and UAV can be defined as the number of collisions per flight hour of UAV as given by

$$P_{\text{event}-3} = P_{\text{aircraft}} = VUW \tag{10}$$

where V is the volume of space swept by the collision box of aircraft in take-off or landing phases, U is the density of UAV operations in airspace, and W is the number of manned aircraft departure/arrival in unit time period.

Figure 5 illustrates a UAV (as a point mass) intruding the collision box of the manned aircraft. The length, width, and height of the collision box are e_l, e_w, e_h respectively.

UAV near airport always operates in low altitude airspace. Thus, we only consider the take-off and landing phases of manned aircraft in our model. The velocity of manned aircraft in such phases can be denoted as

$$v_{\text{A}}(t) = \sigma t + \mu \tag{11}$$

where t is the time, σ is coefficient, and μ is a constant.

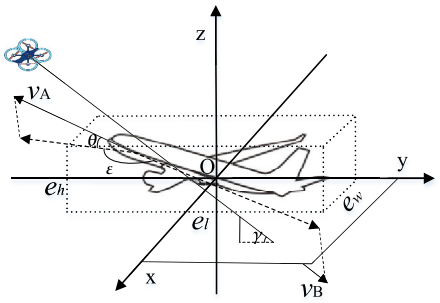

FIGURE 5. Collision model of manned aircraft and UAV.

We next define v_{rh} and v_{rv} as the relative velocities between manned aircraft and UAV in terms of *oxy* coordinate system and *z* axis, which are given respectively by

$$v_{\text{rh}} = \sqrt{(v_{\text{A}}\cos\theta)^2 + (v_{\text{B}}\cos\gamma)^2 + 2v_{\text{A}}\cos\theta v_{\text{B}}\cos\gamma\cos\varepsilon} \tag{12}$$

$$v_{\text{rv}} = v_{\text{A}}\sin\theta - v_{\text{B}}\sin\gamma \tag{13}$$

where θ is the angle between take-off/landing flight path and coordinate system *oxy*, γ is the angle of UAV speed in *oxy axis*, and ε is the projected angle between manned aircraft speed and UAV speed. Assuming the speed direction of UAV is uniform distribution, γ and ε will distribute uniformly in $[-\pi/2, \pi/2]$ and $[0, \pi]$, respectively.

By combining Eq. (12) and Eq. (13), the relative velocity between manned aircraft and UAV is given by

$$\begin{aligned} v_{\text{r}} &= \sqrt{v_{\text{rh}}^2 + v_{\text{rv}}^2} \\ &= \sqrt{v_{\text{A}}^2 + v_{\text{B}}^2 + 2v_{\text{A}}v_{\text{B}}(\cos\theta\cos\gamma\cos\varepsilon - \sin\theta\sin\gamma)} \end{aligned} \tag{14}$$

The average relative velocity $E(v_{\text{r}})$ between manned aircraft and UAV can then be obtained by [30]:

$$E_{v_{\text{r}}} = \frac{\int_0^t \int_{v_{Bmin}}^{v_{Bmax}} \int_{-\frac{\pi}{2}}^{\frac{\pi}{2}} \int_0^{\pi} v_{\text{r}} d\varepsilon d\gamma dv_B dt}{t(v_{Bmax} - v_{Bmin})\pi^2} \tag{15}$$

Assuming that the flight path along with *x* axis, the volume of space V swept by the collision model in Eq. (10) can be expressed as

$$V = e_w e_h \left(E_{v_{\text{r}}} t + e_l\right) \tag{16}$$

D. TOTAL RISK COST MODEL

To evaluate the events after calculating each type of risks, the target level of safety is introduced for each event k, defined as $P_{\text{target}-k}$ and is used as an evaluation standard. The risk level, defined as f_k, can be then obtained as

$$f_k = \frac{P_{\text{event}-k}}{P_{\text{target}-k}} \tag{17}$$

The adjust coefficient ω_k is used to uniformize all risks and the final risk cost for each category is expressed as

$$R_k = \omega_k f_k = \omega_k \frac{P_{\text{event}-k}}{P_{\text{target}-k}} \tag{18}$$

All three types of risk are aggregated as a total risk cost. The total risk cost of a link, consisting of all risks within its safety boundary, is given by

$$R_{total} = \sum_{k=1}^{3} a_k R_k \tag{19}$$

where a_k is the variable and $a_k = \{0, 1\}$. If a particular risk is not in the safety boundary of the link, its cost will not be accounted for the total cost R_{total}. In this case, $a_k = 0$.

IV. COST-EFFECTIVE PATH PLANNING METHOD

In this section, we describe three path planning methods (Dijkstra, A* and ACO) for producing the cost-effective path.

A. PATH PLANNING METHODS

The risk cost map is generated by meshing the areas of concerned and by incorporating their risk cost information. Instead of finding the shortest route, our path planning methods find a cost-effective path that minimizes the total operational risk cost in urban environments. By defining $R_{total(i,j)}$ as the risk cost of box (i, j), the risk cost matrix is

$$\boldsymbol{R} = \begin{bmatrix} R_{total(1,1)} & R_{total(1,2)} & \cdots & R_{total(1,n)} \\ R_{total(2,1)} & R_{total(2,2)} & & R_{total(2,n)} \\ \vdots & & \ddots & \vdots \\ R_{total(m,1)} & R_{total(m,2)} & \cdots & R_{total(m,n)} \end{bmatrix} \tag{20}$$

Then total cost of a path can be calculated as

$$R^L = \sum_{(x,y)\in\Gamma_L} R^L_{total(x,y)} \tag{21}$$

where Γ_L is the set of box areas that the UAV path L travels.

B. MODIFIED A STAR ALGORITHM

Our modified A star (A*) algorithm finds an optimal path with the least risk cost. Standard A* algorithm originates from Dijkstra algorithm, where the heuristic factor is zero. We modified the A* algorithm by devising a novel heuristic function. The heuristic distance used in this function is neither the Manhattan distance nor the Euclidean distance as the risk costs in the map is non-uniformly distributed in each cell. The heuristic distance used in the modified A* is defined as Euclidean distance products a coefficient w_h which equals to the minimal risk cost (>0) in the entire map. The modified cost function is denoted as:

$$f(x) = g(x) + w_h h(x) \tag{22}$$

C. MODIFIED ANT COLONY ALGORITHM

As a global optimization algorithm, ant colony algorithm (ACO) is commonly used in searching the shortest path. We modified the ACO to find a cost-effective path.

To reduce the computational complexity, the ants may not need to search all links in the risk cost map. Ants store pheromones in links and head to those with higher levels of pheromones. In this case, the state transition probability is presented as

$$p_f(g) = \frac{[\tau_f(g)]^{\alpha}(\eta_g)^{\beta}}{\sum_{\delta \epsilon alternative}[\tau_\delta(g)]^{\alpha}(\eta_\delta)^{\beta}}, \quad g = 1, 2, \ldots, g_{max} \tag{23}$$

where g_{max} is the maximum times of iterations, $p_f(g)$ is the probability of path point f been selected at the iteration g, τ_f is the pheromone of path point f, α is the effective factor of pheromone, and β is the effectiveness of heuristic factor. Note that η_f is the heuristic function $\eta_f = 1/C_{ij}$, where C_{ij} is the risk cost between adjacent grid in the risk cost map. Here, *alternative* is the set of path points which can be chosen at next step.

The pheromone is used to connect the solutions in different iterations, as the ants of next iteration will choose their path depend on the pheromone of the current iteration. The pheromone will be updated after all ants completed their searches, and the strategy of pheromone updating is as follows:

$$\tau_f(g+1) = (1-\rho)\tau_f(g) + \Delta\tau_a, \quad f \in \Omega_a \tag{24}$$

where ρ is pheromone evaporation factor, Ω_a is the combination of path points traveled by ant a, and $\Delta\tau_a$ is the increment of pheromone that ant a released on its path. To further enhance the influence of excellent solutions, only the pheromone released by those ants that can successfully reach the destination contributes to the pheromone matrix. Therefore, the increase of pheromone information for ant a is given by

$$\Delta\tau_k = \begin{cases} \dfrac{Q}{C_a}, & \text{ant } a \text{ reached destination} \\ 0, & \text{others} \end{cases} \tag{25}$$

where Q is pheromone constant and C_a is the total risk cost of path that the ant a has traveled.

V. SIMULATION STUDIES

We performed simulations to study and compare three representative urban environments, three path planning methods and four different risk combinations.

A. GENERATION OF RISK COST MAP

A sample urban area of a city in China (20 km × 20 km) is selected in the following simulations. The urban environment consists of eight districts, seventeen main roads, and an aerodrome alert zone. The simulation area covers three flight areas downtown area (blue square), sparse area (green square), and aerodrome area (purple square). The whole area is meshed as the risk cost map ($m \times n = 20 \times 20$ km^2), and the size of each box is 1 km × 1 km as shown in Figure 6.

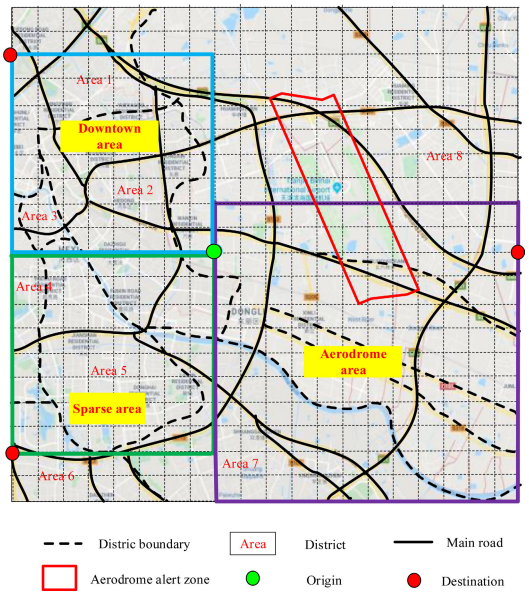

FIGURE 6. City areas (with different flight conditions) considered for simulations.

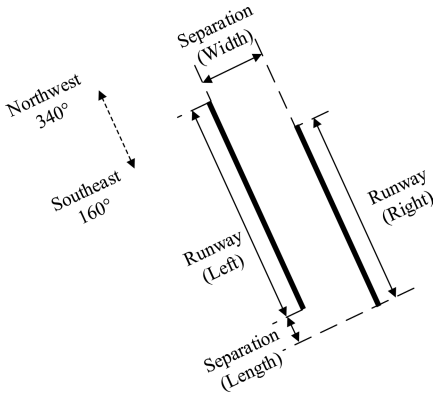

FIGURE 7. The feature of aerodrome (top view).

1) GENERATION OF AERODROME ALERT ZONE

We propose a polygonal alert zone related to approach (precision and non-precision) and departure procedure that considers different runways and their directions. Figure 7 depicts the feature of the aerodrome case.

Minimum Obstacle Clearance (MOC), a safe buffer distance to ensure aircraft fly over obstacles without collisions, is a useful measure in the context of standard instrument departure and precision approach procedure. For non-precision approach procedure, Obstacle Clearance High (OCH) is the minimum high of manned aircraft above the ground.

Figure 8 shows the position relationship between manned aircraft and UAV in take-off and landing phases. Note that UAV can be seen as an obstacle and may exert effect on aircraft's operation, and D is the maximum distance from the runway that might cause manned-unmanned aircraft collision.

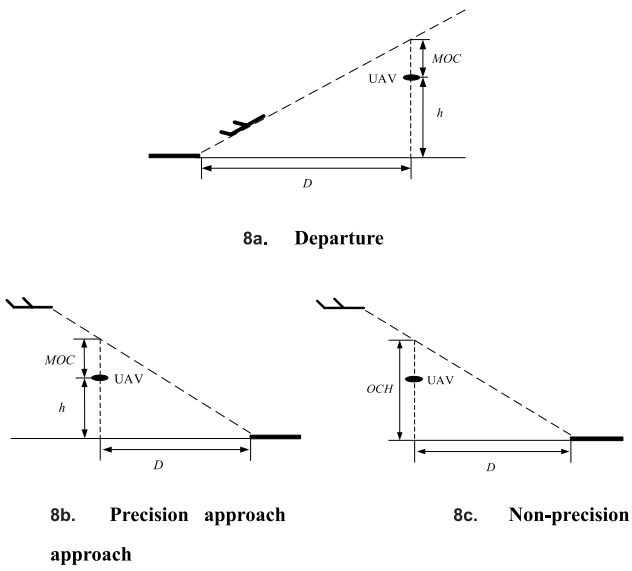

8a. Departure

8b. Precision approach

8c. Non-precision approach

FIGURE 8. Illustration of the position relationship between manned aircraft and UAV in the phases of departure and approach.

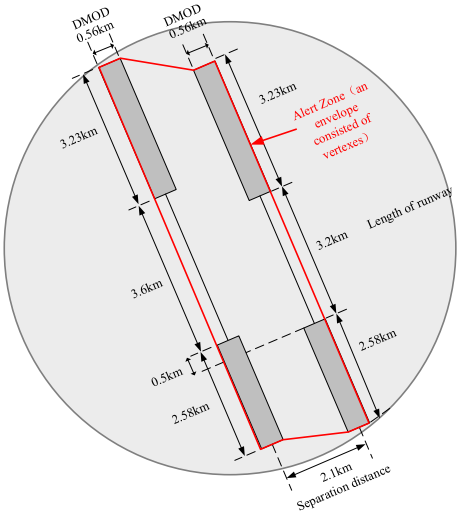

FIGURE 9. Improved aerodrome alert zone (top view).

To obtain a safe value of the length (D) of alert zone along the runway center line, an appropriate value of the height of UAV above the ground is the highest altitude allowed to fly, $h = 60$ m [31]. Then according to the aerodrome's report [32], D in the direction of northwest is 3.23 km while the other side is 2.58 km.

The value of the width of alert zone equals to "DMOD" [33]. DMOD is about 0.56 km around the center of the host aircraft. Commercial aircraft operating within the terminal airspace generally follow a fixed path with little deviation. Therefore, we can consider the center of the host aircraft as the runway extension center line in the phases of approach and departure.

After the analysis above, the boundary of aerodrome alert zone based on the length and width can be obtained, as shown in Figure 9.

The gray circle is the conventional alert area, while the polygon outlined in red is a reduced alert area. In contrast to planners that consider airports as obstacles to entirely avoid, our proposed risk-based method can significantly reduce the aerodrome alert area (see Figure 9) to provide more available airspace (68.81%) for UAV operations. This will enable more area for path planning, reducing the path distance while minimizing the risks.

Our improved aerodrome alert zone increases the efficiency of UAV operations in urban environments with limited low airspace without compromising safety.

2) RISK LEVEL OF PEOPLE, VEHICLE AND AIRPORT AREAS

The basic parameters used in the modelling are (i) gravitational acceleration $g = 9.8$ m/s^2, (ii) air density $\rho_A = 1.225$ kg/m^3, and (iii) performance parameters of DJI Phantom 4 PRO (one of the most commonly used UAVs) [34]: weight $m = 1.38$ kg, maximum UAV operation velocity $v_{\text{Bmax}} = 50$ km/hr, minimum UAV operation velocity $v_{\text{Bmin}} = 12$ km/hr, and incidence of crashing UAV per flight hour $\lambda = 6.04 \times 10^{-5}$ [35].

Table 2 presents the risk level of impact posed to people on the ground. The risk levels are calculated using Eq. (1), Eq. (17), and the parameters in the risk model pertaining to the people on the ground [14], [27], [34], [36] (the exposed area of UAV hitting the ground $A = 0.0188$ m^2, drag coefficient $R_I = 0.3$, impact energy $b = 10^6$ J that might cause 50% fatality as sheltering coefficient $c_s = 0.5$, impact energy threshold $d = 232$ J that can cause fatality as c_s approaching zero).

Table 3 presents the risk level of impact on ground vehicles. This risk level is calculated using Eq. (8), Eq. (17), and related parameters referred from [39]–[42] (vehicle's project area on ground $S_{car} = 9.68$ m^2, traffic density $K = 0.07$ vehicle/m, number of fatalities caused by average traffic accident $T = 0.25$).

Table 4 presents the risk level in aerodrome areas. This risk level is calculated using Eq. (10), Eq. (17), and parameters referred from [30], [44] (the length, width and height of collision box, $e_l = 0.038$km, $e_w = 0.032$km, $e_h = 0.010$km; the coefficient and constant in Eq. (11), $\sigma = 1673$, $\mu = 220$, respectively; the angle between take-off/landing flight path and coordinate system $\theta = \pi/6$ rad; take-off/landing time $t = 0.2$hr; UAV density $U = 3.48 \times 10^{-8}$; number of manned aircraft departure/arrival in unit time period $W = 6$).

3) SENSITIVITY ANALYSIS ON COEFFICIENTS ($\omega_1, \omega_2, \omega_3$)

Based on Eq. (18), the risk cost of each category is dependent upon the coefficients ($\omega_1, \omega_2, \omega_3$). These coefficients represent the weight of each risk category in the total risk cost. This section aims to find out the relationship between the coefficient set ($\omega_1, \omega_2, \omega_3$) and the total risk cost, so as to obtain the optimal coefficient set that minimizes the total risk cost of a planned path.

TABLE 2. Risk level pertaining to people on the ground.

Area	Area 1	Area 2	Area 3	Area 4	Area 5	Area 6	Area 7	Area 8
Population density (10^{-3}people/m^2) [36]	26.62	21.72	27.35	26.41	22.90	1.21	1.53	1.19
$P_{\text{event}-1}$ (10^{-10})	7.7962	6.3612	8.0100	7.7347	6.7067	0.3544	0.4481	0.3485
$P_{\text{target}-1}$ (10^{-6}) [37-38]	1.00	1.00	1.00	1.00	1.00	1.00	1.00	1.00
$f_1 = \frac{P_{\text{event}-1}}{P_{\text{target}-1}}$ (10^{-4})	7.7962	6.3612	8.0100	7.7347	6.7067	0.3544	0.4481	0.3485

TABLE 3. Risk level pertaining to vehicles.

$P_{\text{event}-2}$	2.53×10^{-7}
$P_{\text{target}-2}$[41,43]	1.94×10^{-4}
$f_2 = \frac{P_{\text{event}-2}}{P_{\text{target}-2}}$	1.30×10^{-3}

TABLE 4. Risk level pertaining to aerodrome.

$P_{\text{event}-3}$	2.95×10^{-9}
$P_{\text{target}-3}$[28,45]	1.50×10^{-8}
$f_3 = \frac{P_{\text{event}-3}}{P_{\text{target}-3}}$	1.97×10^{-1}

The risk cost posed to manned aircraft is the significant factor compared with that to people and vehicles on the ground, as the risk level pertaining to airport has a larger order of magnitude than that to people and vehicles (see Tables 2, 3, 4). The planned path must not enter airport area once the risk cost of airport exceeds its threshold which is dependent upon the coefficient ω_3. Therefore, the ω_3 will be first analyzed and determined while keeping ω_1 and ω_2 constant.

Assuming $\omega_1 = \omega_2 = 100$, the value interval of ω_3 is set as $[1\times10^{-3}: 5\times10^{-2}]$ based on its order of magnitude. The step size of ω_3 is 1×10^{-3}. For each set, the input is the set of $(1, 1, \omega_{3_i})$ and the output is the set $(1, 1, \omega_{3_i}, R_{(total)_i})$. R_{total} will be different due to the following two factors:

- **a.** Combination factor: The different combination of the coefficients $(\omega_1, \omega_2, \omega_3)$ may leads to different optimal path, and that (sensitivity) will result in a different R_{total};
- **b.** Scaling factor: The scale of individual coefficients will also lead to different R_{total} for each set in same flight conditions (same OD pairs).

Next, we investigate the sensitivity of the combination factor (factor **a**) by excluding the influence of scaling factor (factor **b**) and by proposing the following equation:

$$R_{total(i,j)} = \sum_i \sum_j \left(\frac{\omega_1 R_{1(i,j)}}{\zeta_1} + \frac{\omega_2 R_{2(i,j)}}{\zeta_2} + \frac{\omega_3 R_{3(i,j)}}{\zeta_3}\right) \quad (26)$$

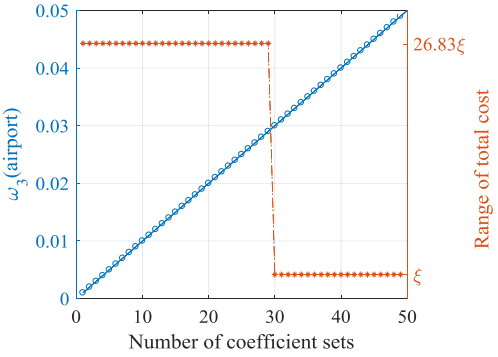

FIGURE 10. Threshold of airport coefficient ω_3.

where $\zeta_1, \zeta_2, \zeta_3$ are adjustment coefficients, which are proportional to the increased amount of related cost ($\omega_i R_i$) due to the change of the coefficients. By assuming the adjustment coefficients $\zeta_1, \zeta_2, \zeta_3$ equal respectively to $\omega_1, \omega_2, \omega_3$, the coefficient ω_3 can be obtained as shown in Figure 10.

Figure 10 illustrates a clear threshold ($\omega_3 = 0.03$) where the total risk cost significantly changes from 26.83ξ to ξ (ξ is the unit of total risk cost). Below the threshold, the total risk cost remains high because the planned path entered the airport area, causing the increase in risk. On the other hand, when ω_3 exceeds the threshold, the risk cost of airport area will be too great to allow any planned path to enter. Instead, the planned path will go through low risk areas outside the airport to lessen the total risk cost. In this case, the threshold of the coefficient ratio is $\omega_1{:}\omega_2{:}\omega_3 \approx 3333{:}3333{:}1$ – the path must not enter airport area as long as ω_1 and ω_2 are less than 3333 times of ω_3.

Next, assuming $\omega_3 = 1$, the total risk cost can be evaluated by using Eq. (26), given ω_1 and ω_2. Assume the coefficients of people and vehicle to be $\omega_1 = [1{:}100]$ and $\omega_2 = [1{:}20]$, while the step size of them to be 5 and 1, respectively. For each set, the input is $(\omega_{1_i}, \omega_{2_i}, 1)$ and the output is $(\omega_{1_i}, \omega_{2_i}, 1, R_{(total)_i})$. The result is illustrated in Figure 11.

Figure 11 shows that the total cost decreases with (i) an increase in the people risk coefficient and (ii) a decrease in the vehicle risk coefficient. There is a significant linear relationship between ω_1 and ω_2 (see the line in the concave area), which generates the lowest total cost value. The linear relationship is $\omega_1/\omega_2 = 15$. Therefore, we use the coefficient

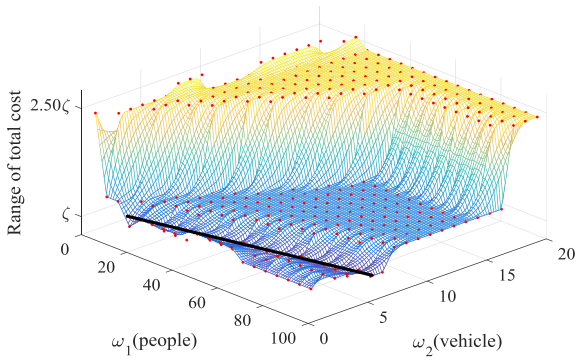

FIGURE 11. Relationship of total risk cost with coefficients ω_1 and ω_2.

set $(\omega_1, \omega_2, \omega_3) = (1.5 \times 10^5, 1 \times 10^4, 1 \times 10^2)$ as the optimized set for the risk cost computations in the following sections.

B. UAV COST-EFFECTIVE PATH PLANNING BASED ON RISK COST MAP

To investigate the feasibility and effectiveness of the proposed risk assessment method, we performed two groups of simulations. First, we conducted risk-based UAV path planning in different flight areas (downtown, sparse, aerodrome) to validate that the proposed models can be applied in diverse urban environments. The performance of the three algorithms under the same simulation environments were compared in terms of computational time and quality of paths. Second, we performed simulations in same flight areas where the risk cost map varies based on different combination and number of involved risks. This allows us to analyze the influence of different risk combinations on the total risk cost.

1) PATH PLANNING IN DIFFERENT URBAN ENVIRONMENTS

We conducted simulations in three representative urban environments: downtown area, sparse area (suburban area), and aerodrome area. Based on that, three missions were planned. The end points are located in three directions representing paths to different urban environments. To eliminate the influence of differing initial distance on the final path, the shortest distance from start point to the three end points are the same in this study.

In each environment, three algorithms (Dijkstra, modified A*, and modified ACO) are used to produce the cost-effective path. The basic settings of these algorithm are given as follows:

1) Standard Dijkstra with no modification;
2) Modified A* by defining a heuristic distance as Euclidean distance products a coefficient which equals to the minimal risk cost (>0) in the entire map.
3) Ant Colony algorithm settings: population size of 20, pheromone attenuation coefficient of 0.2, pheromone constant of 100, the effectiveness of pheromone and heuristic factor of 1, and maximum number of iterations of 100.

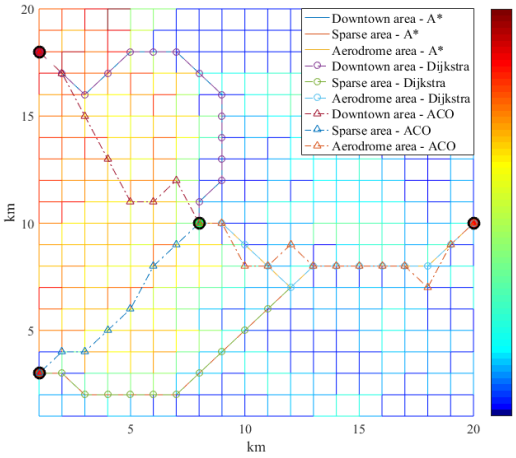

FIGURE 12. Simulation results of different flight areas.

TABLE 5. Cost-effective path planning results.

Environments	Total risk cost			Computational time (s)		
	Dijkstra	A*	ACO	Dijkstra	A*	ACO
Downtown	666.90	666.90	672.13	4.95	2.44	1.21
Sparse	217.77	217.77	295.59	3.72	2.51	1.01
Aerodrome	127.73	127.73	151.19	4.01	2.72	1.56

TABLE 6. Average results of 50 independent runs of modified ACO.

Average value	Downtown	Sparse	Aerodrome
Total risk cost	710.45	336.62	163.54
Computational time (s)	1.54	1.25	2.01

Figure 12 and Table 5 show the computational time and total risk cost of the three algorithms in different flight areas. Note that due to the randomization of ACO path planning process, we performed 50 parallel simulations and selected the best solution as presented in Figure 12 and Table 5.

To demonstrate the robustness of modified ACO algorithm, 50 parallel simulations for three different cases were performed and the results obtained are tabulated in Table 6.

The total costs in the downtown area are the highest among all three algorithms, while the total costs in the aerodrome area are the lowest. Downtown areas have high density of people and vehicles on the ground with hardly any low risk area for UAVs to operate, resulting in a high total risk. In aerodrome areas, although the collision risk in airport airspace is high, none of the generated paths entered the aerodrome. The paths are outside the aerodrome where there are lower risks of impacting people and ground vehicles. In sparse areas, the total cost is slightly higher than that of aerodrome area.

Comparing the three algorithms, Dijkstra and modified A* both found the lowest risk cost path (having same total risk cost), while modified A* has about half the computational

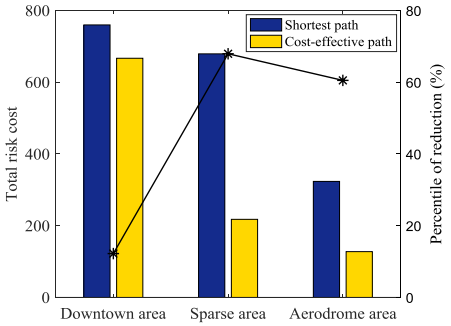

FIGURE 13. Total risk cost is compared among the shortest paths and cost-effective paths using modified A* algorithm.

TABLE 7. Total risk cost of different paths.

Path	Path A	Path B	Path C	Path D
Total risk cost	1531.30	974.64	919.88	855.29

time of Dijkstra. Modified ACO took the least time, but its performance in producing the cost-effective path is the worst, especially in sparse and aerodrome areas, with twice the total risk cost of its path compared to other two algorithms. Therefore, we used the modified A* algorithm in the following path planning studies.

Figure 13 compares the total risk cost of the cost-effective paths using the modified A* algorithm and shortest paths in the three different urban environments.

In all environments, the path generated by the cost-effective path planning method using the modified A* algorithm outperforms the one obtained by the distance-based method. Modified A* considers risk cost when performing path planning and avoids high risk cost areas, while the distance-based does not and may enter high risk cost areas.

2) UAV PATH PLANNING WITH DIFFERENT RISK COMBINATIONS

To further understand the influence of risks involved on the risk cost map and path planning, we conducted simulations in the same flight areas but with different combinations of risk types.

Four paths are studied in the simulations: (i) Path A considers vehicle and airport, (ii) Path B considers people and airport areas, (iii) Path C considers people and vehicles, and (iv) Path D consider all three risks. Figure 14 and Table 7 present the simulation results of the four paths.

Path D, which considers all three risks types, is the most cost-effective path. It has a total risk cost of 855.29. Path A is the worst, with a 79.04% higher total risk cost than Path D. As Path A does not consider the people risk in the path planning, the UAV enters densely populated area where the risk cost is very high. The risk costs of Path B and Path C are similar; Path B's total risk cost is 5.95% higher than Path C's.

To further understand the differences between these paths in terms of risk cost, we studied each risk cost (people risk

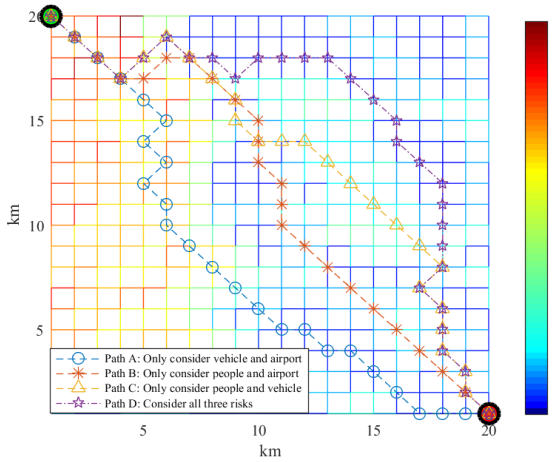

FIGURE 14. Flight paths considering different combination of risks.

TABLE 8. Comparisons of each risk cost of different paths.

Risk type not considered in the path	R_1(Path A)	R_2 (Path B)	R_3(Path C)
Risk cost	1440.30	234.00	98.50
Risk cost in Path D	660.29	195.00	0
Percentile of reduction %	54.16	16.67	100

cost R_1, vehicle risk cost R_2, and airport risk cost R_3) in different paths. The results are shown in Table 8.

Let's take Path C as an example. This path does not consider the risk associated with airports. The UAV path entered the airport area, resulting in an airport risk cost R_3 of 98.50. On the contrary, Path D planning uses a risk map that includes airport risk, thereby avoiding this high-risk cost area, resulting in an airport risk cost of 0.

Paths A and B do not consider people risk and vehicle risk respectively, which leads to a high risk of the two ignored risk categories.

VI. CONCLUDING REMARKS

A risk assessment model and a method for risk-based path planning in urban environments have been proposed and presented in this paper. To validate our proposed method, we performed various simulations with different scenarios and path search algorithms.

Our key findings are summarized below:

(1) Our proposed total risk assessment model quantitatively incorporates and represents risk distribution situations in urban environments to provide risk data for UAV path planning.

(2) Our risk-cost method generates cost-effective path for safe UAV operations in urban environments.

(3) The risk cost pertaining to downtown areas is the highest, followed by that of sparse area and airport area. It makes sense because the route changing of drone operations

in downtown areas is less flexible than that surrounding the airport area. Note that the influence of risks on path planning in other urban environments can be different due to different risk contributions to the cost map.

(4) Modified A* performs the best in finding a path with the lowest risk cost within a reasonable computational time frame. ACO takes the least time finding a relatively low-risk path so it can be used for time-sensitive cases.

(5) Better path planning results are achieved when considering more risk types in the total risk assessment model. To evaluate the total risk, other risk sources (for example, convective weather) can be incorporated in the risk cost map. Our proposed methodology can be extended to more complex urban environments by incorporating other relevant parameters and data in future work.

ACKNOWLEDGMENT

The authors would like to express their gratitude to Dr. Yuandi Zhao, Dr. Yu Wu and UAS team in the NTU-ATMRI for their valuable feedback and suggestions to this work.

REFERENCES

[1] R. Reshma, T. Ramesh, and P. Sathishkumar, "Security situational aware intelligent road traffic monitoring using UAVs," in *Proc. Int. Conf. VLSI Syst., Archit., Technol. Appl. (VLSI-SATA)*, Jan. 2016, pp. 1–6.

[2] C. Thiel and C. Schmullius, "Comparison of UAV photograph-based and airborne LiDAR-based point clouds over forest from a forestry application perspective," *Int. J. Remote Sens.*, vol. 38, nos. 8–10, pp. 2411–2426, May 2017.

[3] P. Kopardekar. (2019). Urban air mobility regional readiness. NASA. [Online]. Available: https://ntrs.nasa.gov/search.jsp?R=20190032255

[4] H. Menouar, I. Guvenc, K. Akkaya, A. S. Uluagac, A. Kadri, and A. Tuncer, "UAV-enabled intelligent transportation systems for the smart city: Applications and challenges," *IEEE Commun. Mag.*, vol. 55, no. 3, pp. 22–28, Mar. 2017.

[5] F. Qi, X. Zhu, G. Mang, M. Kadoch, and W. Li, "UAV network and IoT in the sky for future smart cities," *IEEE Netw.*, vol. 33, no. 2, pp. 96–101, Mar. 2019.

[6] B. Levasseur, S. Bertrand, N. Raballand, F. Viguier, and G. Goussu, "Accurate ground impact footprints and probabilistic maps for risk analysis of UAV missions," in *Proc. IEEE Aerosp. Conf.*, Mar. 2019, pp. 1–10.

[7] F. L. L. Medeiros and J. D. S. D. Silva, "Computational modeling for automatic path planning based on evaluations of the effects of impacts of UAVs on the ground," *J. Intell. Robot. Syst.*, vol. 61, nos. 1–4, pp. 181–202, Jan. 2011.

[8] Z. Zhang, J. Zhang, P. Wang, and L. Chen, "Research on operation of UAVs in non-isolated airspace," *Comput., Mater. Continua*, vol. 57, no. 1, pp. 151–166, 2018.

[9] M. Maiouak and T. Taleb, "Dynamic maps for automated driving and UAV geofencing," *IEEE Wireless Commun.*, vol. 26, no. 4, pp. 54–59, Aug. 2019.

[10] Q. Tan, Z. Wang, Y.-S. Ong, and K. H. Low, "Evolutionary optimization-based mission planning for UAS traffic management (UTM)," in *Proc. Int. Conf. Unmanned Aircr. Syst. (ICUAS)*, Jun. 2019, pp. 952–958.

[11] A. Donkels, "Trajectory risk evaluation for autonomous low-flying air transport," *J. Guid., Control, Dyn.*, vol. 43, no. 5, pp. 1026–1033, May 2020.

[12] B. Pang, Q. Tan, and K. H. Low, "A risk-based UAS traffic network model for adaptive urban airspace management," in *Proc. AIAA Aviation Forum*, 2020, p. 2900, doi: 10.2514/6.2020-2900.

[13] S. Primatesta, G. Guglieri, and A. Rizzo, "A risk-aware path planning strategy for UAVs in urban environments," *J. Intell. Robot. Syst.*, vol. 95, no. 2, pp. 629–643, Aug. 2019.

[14] S. Primatesta, A. Rizzo, and A. L. Cour-Harbo, "Ground risk map for unmanned aircraft in urban environments," *J. Intell. Robot. Syst.*, vol. 97, pp. 489–509, May 2019.

[15] P. P.-Y. Wu, D. Campbell, and T. Merz, "Multi-objective four-dimensional vehicle motion planning in large dynamic environments," *IEEE Trans. Syst. Man, Cybern. B, Cybern.*, vol. 41, no. 3, pp. 621–634, Jun. 2011.

[16] Z. Wu, J. Li, J. Zuo, and S. Li, "Path planning of UAVs based on collision probability and Kalman filter," *IEEE Access*, vol. 6, pp. 34237–34245, 2018.

[17] H. Jiang and Y. Liang, "Online path planning of autonomous UAVs for bearing-only standoff multi-target following in threat environment," *IEEE Access*, vol. 6, pp. 22531–22544, 2018.

[18] H. Hu, Y. Wu, J. Xu, and Q. Sun, "Cuckoo search-based method for trajectory planning of quadrotor in an urban environment," *Proc. Inst. Mech. Eng., G, J. Aerosp. Eng.*, vol. 233, no. 12, pp. 4571–4582, Sep. 2019.

[19] J. D. S. Arantes, M. D. S. Arantes, C. F. M. Toledo, O. T. Júnior, and B. C. Williams, "Heuristic and genetic algorithm approaches for UAV path planning under critical situation," *Int. J. Artif. Intell. Tools*, vol. 26, no. 1, Feb. 2017, Art. no. 1760008.

[20] E. Rudnick-Cohen, J. W. Herrmann, and S. Azarm, "Risk-based path planning optimization methods for unmanned aerial vehicles over inhabited areas," *J. Comput. Inf. Sci. Eng.*, vol. 16, no. 2, Jun. 2016, Art. no. 021004.

[21] E. W. Dijkstra, "A note on two problems in connexion with graphs," *Numerische Math.*, vol. 1, no. 1, pp. 269–271, Dec. 1959.

[22] Y. Li, Y. Wu, X. Su, and J. Song, "Path planning for aircraft fleet launching on the flight deck of carriers," *Mathematics*, vol. 6, no. 10, p. 175, Sep. 2018.

[23] P. Yao and S. Zhao, "Three-dimensional path planning for AUV based on interfered fluid dynamical system under ocean current (June 2018)," *IEEE Access*, vol. 6, pp. 42904–42916, 2018.

[24] L. E. Kavraki, P. Svestka, J.-C. Latombe, and M. H. Overmars, "Probabilistic roadmaps for path planning in high-dimensional configuration spaces," *IEEE Trans. Robot. Autom.*, vol. 12, no. 4, pp. 566–580, Aug. 1996.

[25] S. LaValle. (1998). *Rapidly-Exploring Random Trees: A New Tool for Path Planning*. [Online]. Available: http://citeseerx.ist.psu.edu/viewdoc/download?doi=10.1.1.35.1853&rep=rep1&type=pdf

[26] M. Dorigo and L. M. Gambardella, "Ant colony system: A cooperative learning approach to the traveling salesman problem," *IEEE Trans. Evol. Comput.*, vol. 1, no. 1, pp. 53–66, Apr. 1997.

[27] C. H. Koh, K. H. Low, L. Li, Y. Zhao, C. Deng, S. K. Tan, Y. Chen, B. C. Yeap, and X. Li, "Weight threshold estimation of falling UAVs (unmanned aerial vehicles) based on impact energy," *Transp. Res. C, Emerg. Technol.*, vol. 93, pp. 228–255, Aug. 2018.

[28] K. Dalamagkidis, K. P. Valavanis, and L. A. Piegl, "Evaluating the risk of unmanned aircraft ground impacts," in *Proc. 16th Medit. Conf. Control Automat.*, Jun. 2008, pp. 709–716.

[29] *European Drones Outlook Study-Unlocking the Value for Europe*, SESAR Joint Undertaking, Brussels, Belgium, 2016.

[30] Y. Gao and D. Liu, "Research on model for aircraft collision risk in terminal area after low altitude open," (in Chinese), *China Saf. Sci. J.*, vol. 24, no. 6, pp. 141–145, 2014.

[31] *UA Safety Guidelines*. Accessed: Jun. 1, 2020. [Online]. Available: https://www.caas.gov.sg/public-passengers/unmanned-aircraft/ua-safety-guidelines

[32] *Aeronautical Information Publication, Tianjin Binhai International Airport*, (in Chinese), Aeronaut. Inf. Service Center, Air Traffic Manage. Bur., Civil Aviation Authority China, Beijing, China, 2020.

[33] C. H. J. Wang, S. K. Tan, and K. H. Low, "Collision risk management for non-cooperative UAS traffic in airport-restricted airspace with alert zones based on probabilistic conflict map," *Transp. Res. C, Emerg. Technol.*, vol. 109, pp. 19–39, Dec. 2019.

[34] *Products Brochure*. Accessed: Jan. 23, 2020. [Online]. Available: https://www.dji.com/cn/products/compare-consumerdrones?site=brandsite&from=landing_page

[35] S. K. Yan, "Evaluating the risk of unmanned aircraft operation," (in Chinese), Civil Aviation Univ. China, Tianjin, China, 2018.

[36] *Tianjin Introduction*. (in Chinese). Accessed: Jun. 1, 2020. [Online]. Available: https://baike.baidu.com/item/%E5%A4%A9%E6%B4%A5/132308?fromtitle=%E5%A4%A9%E6%B4%A5%E5%B8%82&fromid=213824#5

[37] Z. J. Zhang and S. G. Zhang, "Estimated method of target level of safety for unmanned aircraft system," (in Chinese), *J. Aerosp. Power*, vol. 33, no. 4, pp. 1017–1024, 2018.

[38] R. Clothier, R. Walker, and N. Fulton, "A casualty risk analysis for unmanned aerial system (UAS) operations over inhabited areas," in *Proc. 2nd Australas. Unmanned Air Vehicles Conf. (AIAC)*, 2007, pp. 1–16.

[39] Q. Sun, W. Zhang, L. Wan, and X. Wang, "Analysis of vehicle dimension definition and proportion of coordination in Chinese market," SAE Tech. Paper 2015-01-0477, 2015.
[40] X. Lin and J. Xu, "Macroscopic fundamental diagram estimation fusion method of road networks based on adaptive weighted average," (in Chinese), *J. Transp. Syst. Eng. Inf. Technol.*, vol. 18, no. 6, pp. 102–109, 2018.
[41] *Statistical Bulletin of the People's Republic of China on the 2016 National Economic and Social Development*. (in Chinese). Accessed: Jun. 28, 2020. [Online]. Available: http://www.stats.gov.cn/tjsj/zxfb/201702/t20170228_1467424.html
[42] *The News of Road Traffic Accidents of China*. (in Chinese). Accessed: Jun. 18, 2020. [Online]. Available: http://www.mps.gov.cn/n2255079/n2256030/n2256031/c5605650/content.html
[43] *The Profile of China*. (in Chinese). Accessed: Apr. 22, 2020. [Online]. Available: http://www.gov.cn/guoqing/index.htm
[44] *General and Small Aviation Operation Situation in 2018*, (in Chinese), Flight Standards Dept. Civil Aviation Admin. China, Beijing, China, Feb. 2019.
[45] *Target Level of Sefety*. (in Chinese). Accessed: Jan. 26, 2020. [Online]. Available: http://www.caac.gov.cn/ztzl/RDZT/MHGGKF/WKGGKFXCJ/201811/t20181126_193168.html

XINTING HU is currently pursuing the master's degree majoring in transportation planning and management with the Civil Aviation University of China. Her research interests include urban airspace management and UAS traffic management (UTM). She is currently involved in risk assessment for UAV operations in urban environments.

BIZHAO PANG received the bachelor's degree and the master's degree in transportation science and engineering from the Civil Aviation University of China, in 2016 and 2019, respectively. He has been a Research Associate with the Air Traffic Management Research Institute (ATMRI), Nanyang Technological University (NTU). His research interest includes unmanned aircraft systems (UAS).

FUQING DAI received the bachelor's degree from Nanjing University, China, and the master's degree from the Ecole Nationale de l'Aviation Civile, France. He currently holds the Dean's Chair at the Air Traffic Management School, Civil Aviation University of China. He is also a Professor focusing on the research of airspace planning and management, flight procedures design and optimization, and UTM and ATM systems.

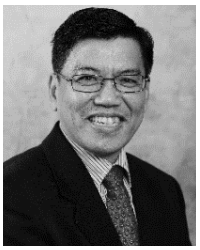

KIN HUAT LOW (Member, IEEE) received the B.Sc. degree from National Cheng Kung University, Taiwan, and the M.Sc. and Ph.D. degrees in mechanical engineering from the University of Waterloo, Canada. He is currently a Professor with the School of Mechanical and Aerospace Engineering, Nanyang Technological University (NTU), Singapore. He has authored or coauthored about 400 journal articles and conference papers in the areas of robotics, biomimetics and rehabilitation robotics, unmanned aerial vehicles, air traffic management, impacts, power transmission systems, and structural dynamics and vibrations. He is in charge of the UAS Programme at the NTU's Air Traffic Management Research Institute (ATMRI). The ATMRI's UAS team has successfully organized the first International Conference on Air Mobility with Unmanned Systems and Engineering (AMUSE), in July 2020. He is also an Honorary Member of the Global UTM Association (GUTMA).